J Appl Electrochem (2010) 40:1545–1553
DOI 10.1007/s10800-010-0132-8

ORIGINAL PAPER

Effect of electrolyte concentration on morphology, microstructure and electrochemical impedance of anodic oxide film on titanium alloy Ti-10V–2Fe–3Al

Jianhua Liu · Junlan Yi · Songmei Li · Mei Yu · Guolong Wu · Liang Wu

Received: 9 July 2009 / Accepted: 3 April 2010 / Published online: 26 May 2010

Abstract Anodic oxide films were fabricated on titanium alloy Ti-10V–2Fe–3Al in ammonium tartrate solutions at the concentrations: 1, 3, 5, 10 and 15 g L^{-1}. The morphological characteristics and microstructures of the films of the alloy were studied by optical microscopy (OM) and Raman spectroscopy (Raman), respectively. The electrochemical impedances of the films in 0.5 mol L^{-1} H_2SO_4 solution were investigated by electrochemical impedance spectroscopy (EIS). It was showed that different electrolyte concentrations led to different change rates of anodizing forming voltage. The change rate significantly affected the morphology, microstructure and electrochemical impedance of anodic oxide film. When electrolyte concentration was 5 g L^{-1}, anodic oxide film was the most uniform, exhibited by the least and smallest breakpoints on the film. In addition, the amount of crystal phase of the film was the largest at 5 g L^{-1}, showed by the highest intensity of Raman peaks. Furthermore, the electrochemical impedance of the film of the alloy was the greatest at 5 g L^{-1}, demonstrated by the highest values of polarization resistances and lowest values of capacitances. These phenomenon were associated with the minimum value of the change rate of anodizing forming voltage at 5 g L^{-1}.

Keywords Titanium alloy · Electrolyte concentration · Electrochemical impedance spectroscopy · Raman spectroscopy

Abbreviations

OM	Optical microscopy
Raman	Raman spectroscopy
EIS	Electrochemical impedance spectroscopy
WE	The work electrode
CE	The counter electrode
RE	The reference electrode
SCE	Saturated calomel electrode
AC	Alternating current
R_S	The solution resistance
Q_{pL}	The capacitance of the porous layer
R_{pL}	The polarization resistance of the porous layer
Q_{bL}	The capacitance of the barrier layer
R_{bL}	The polarization resistance of the barrier layer
Q	The magnitude of CPE
Z_{CPE}	The impedance of the constant-phase element
n	The exponent of CPE
ω	The angular frequency
Z_{pLCPE}	The impedance of the constant-phase element of the porous layer
Z_{bLCPE}	The impedance of the constant-phase element of the barrier layer
n_b	The exponent of CPE of the barrier layer
n_p	The exponent of CPE of the porous layer
i	The ionic current
A	The electrolytic constants
B	The electrolytic constants
E	The electric field strength
V	The anodizing forming voltage
δ	The anodic oxide thickness
α	The growth constant

J. Liu (✉) · J. Yi · S. Li · M. Yu · G. Wu · L. Wu
School of Materials Science and Engineering,
Beihang University, Beijing 100191, China
e-mail: liujh@buaa.edu.cn

1 Introduction

Owing to its high strength to weight ratio, great fracture toughness and outstanding corrosion resistance, titanium

alloy Ti-10V–2Fe–3Al has been a promising material in aerospace industry [1–3]. The favorable corrosion resistance of such titanium alloy should be attributed to the oxide film naturally formed on its surface [4]. Corrosion is believed to occur through "weak spots" in the natural oxide film. A forced increase in film thickness would eliminate such weak spots and increase the corrosion resistance. Anodizing is commonly used to increase the thickness and the corrosion resistance of the film on titanium substrate [5].

Electrochemical parameters of anodizing significantly affect the growth behavior and properties of anodic oxide films formed on the titanium metal [6]. However, results reported in the literatures were rather complex and somewhat contradictory on the electrochemical growth behavior and properties of anodic oxide films [7–10]. Disagreements between various studies may arise from varying surface preparations and anodizing parameters. The parameters that most affect the oxide characteristics are the electrolyte solution (concentration of reagents), the anodic current density imposed and the electrolyte temperature [9, 11]. Most of the studies were focused on the pure titanium. To our best knowledge, there is no report about anodizing parameters and growth behaviors of anodic oxide films formed on titanium alloy Ti-10V–2Fe–3Al.

In our previous paper, thick, uniform and non-transparent anodic oxide films were fabricated on titanium alloy Ti-10V–2Fe–3Al without using hydrofluoric acid or fluoride [12]. The present work is to evaluate the effect of electrolyte concentration on formation of anodic oxide films of titanium alloy Ti-10V–2Fe–3Al. The relation curves of anodizing forming voltage and anodizing time of specimens at various electrolyte concentrations were analyzed. Surface morphologies, microstructures and electrochemical impedances of anodic oxide films were investigated by optical microscopy (OM), Raman spectroscopy (Raman) and electrochemical impedance spectroscopy (EIS), respectively. Correlations among electrolyte concentration, anodizing kinetics, surface morphology, microstructure and electrochemical impedance of anodic oxide film were revealed.

2 Experimental

2.1 Specimen preparation

A forged block of titanium alloy Ti-10V–2Fe–3Al was cut into 100 mm × 30 mm × 3 mm sheets. The nominal chemical components of titanium alloy Ti-10V–2Fe–3Al are shown in Table 1. Each specimen was abraded with silicon carbide paper of successive grades from 300 to 600 grit, then rinsed with acetone and deionized water, and finally dried in the air.

Table 1 Nominal chemical components of titanium alloy Ti-10V–2Fe–3Al (wt%)

V	Fe	Al	C	N	0	Ti
10.100	2.100	3.100	<0.050	<0.050	<0.130	Balance

Anodizing was carried out in a cell with a thermostat water bath and a magnetic stirring apparatus. The specimen was used as the anode and a 1Cr18Ni9Ti stainless steel plate was used as the cathode. The electrolyte used was an aqueous solution of ammonium tartrate, which was prepared by analytical grade chemicals and deionized water.

A pulse galvanostatic power supply WMY-IV was employed. The applied voltage, current, duty ratio, frequency of the power supply were continuously adjustable in the ranges of 0–250 V, 0–10 A, 10–80% and 0.067–2 Hz, respectively. The pulse of the power supply was unidirectional and exhibited a square wave. Specimens were anodized in ammonium tartrate solution at the concentrations: 1, 3, 5, 10 and 15 g L^{-1}, respectively. Other main parameters of anodizing are fixed and shown in Table 2. More detail fabrication conditions were studied in previous [12, 13].

2.2 Surface analysis

The surface morphologies of the anodized specimens were observed by an optical microscope (OM, Olympus-BX51M). The microstructures of anodic oxide films were determined by a Raman spectroscope (Raman, Yvon Jobin Horiba-HR800, using a He–Ne laser without filter, 633 nm).

2.3 Electrochemical measurement

The EIS measurements for each anodized specimen were carried out using a potentiostat/galvanostat (Parstat 2273, Princeton Applied Research) in a homemade three-electrode electrochemical arrangement in 0.5 mol L^{-1} H_2SO_4 solution at 25 ± 3 °C.

The schematic diagram of the electrochemical arrangement is shown in Fig. 1. The anodized sheet specimen was

Table 2 Parameters of anodizing process

Parameters	Value (unit)
Current density	10 A dm^{-2}
Duty ratio	30%
Frequency	1.67 Hz
Temperature	15 ± 2 °C
Agitation speed	100 rpm
Anodizing time	30 min
Surface area ratio of cathode to anode	4:1

used as the work electrode (WE) and compressed tightly to the wall of the cell by threaded bolts and nuts. The diameter of the hole on the wall of the cell was 20 mm. The washer was used as the air-tight seal which controlled the experimental area of the sheet specimen ($S = \pi(d/2)^2 \approx 3.14159\ cm^2$) straightly. A pure platinum sheet was used as the counter electrode (CE) and a saturated calomel electrode (SCE) was used as the reference electrode (RE). Specimens were immersed in the sulfuric acid solution at open circuit condition for 30 min prior to the EIS tests. The alternating current (AC) impedance spectra of specimens were obtained at the open circuit potential, with an amplitude of 10 mV and a scan frequency range of 100 kHz–10 mHz (10 points per decade). Nyquist and Bode plots were obtained by curve fitting using a commercial software package called Electrochemistry Power Suite™. The EIS spectra were simulated using the Zsimpwin simulation software.

3 Results

3.1 Anodizing forming behavior of specimens at various electrolyte concentrations

Figure 2 shows anodizing forming voltage with anodizing time relation curves of specimens at various electrolyte concentrations. The anodizing process was divided into three steps in all tested solutions: (1) anodizing forming voltage went up linearly with time to a certain point (maximum anodizing forming voltage); (2) anodizing forming voltage decreased gradually with anodizing time; (3) anodizing forming voltage approximately kept steady. The detail results of anodizing forming voltage obtained at various electrolyte concentrations are recorded in table.

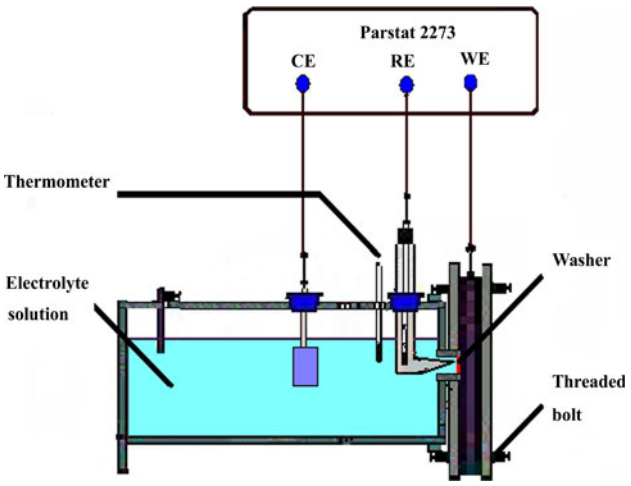

Fig. 1 Schematic diagram of homemade three-electrode electrochemical arrangement

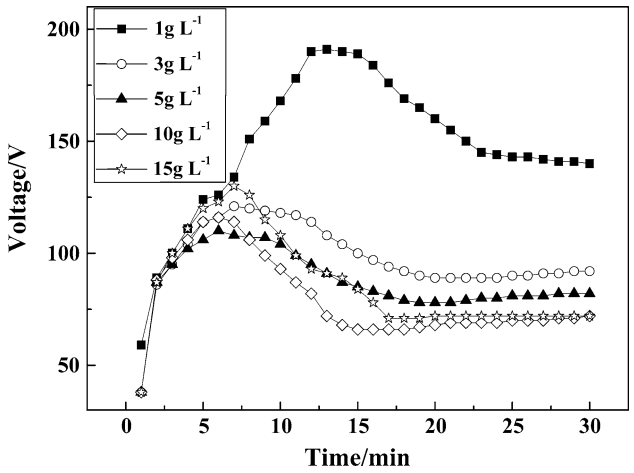

Fig. 2 Anodizing forming voltage with anodizing time relation curves of specimens at various electrolyte concentrations

As presented in Table 3, the maximum value, ultimate value, decreasing amplitude (the difference between the maximum value and ultimate value) and change rate of anodizing forming voltage decreased with electrolyte concentration until they reached the minimum at 5 g L^{-1}. Thereafter, all these values increased with electrolyte concentration. It was evident that the falling rate of anodizing forming voltage in step (2) was the largest at 10 g L^{-1}. The steady time in step (3) was the least at 1 g L^{-1}.

3.2 Morphology of specimens at various electrolyte concentrations

The optical images of the specimens at various electrolyte concentrations are presented in Fig. 3a–e. Breakdown points were clearly seen on all the specimens with different colors. Breakdown points on anodic oxide film formed at 10 g L^{-1} (d) were obviously larger in size and more in amount than those at other concentrations. The most uniform morphology with the least and smallest breakdown points was investigated at 5 g L^{-1} (c). The porous layers of anodic oxide films formed at various electrolyte concentrations exhibited the same color (yellow), whereas the porous layer was the thinnest at 1 g L^{-1} (a).

3.3 Microstructure of specimens at various electrolyte concentrations

Figure 4 gives the Raman spectra of anodic oxide films formed on titanium alloy Ti-10V–2Fe–3Al at various electrolyte concentrations. The peaks of anodic oxide films of the tested specimens and those related to crystal phases of anodic oxide films reported in literature [14], are listed in Table 4. The intensity of the peaks increased with

Table 3 Results of anodizing forming voltage obtained at various electrolyte concentrations

Electrolyte concentration (g L^{-1})	Maximum value (V)	Ultimate value (V)	Decreasing amplitude (V)	Change rate		Steady time in step (3) (min)
				Raising rate in step (1) (V min^{-1})	Falling rate in step (2) (V min^{-1})	
1	191	140	51	24.8	3.6	4
3	121	91	30	22.8	2.5	12
5	110	82	28	20.4	2.3	12
10	116	72	44	22.8	11.6	15
15	130	72	58	24.0	5.8	14

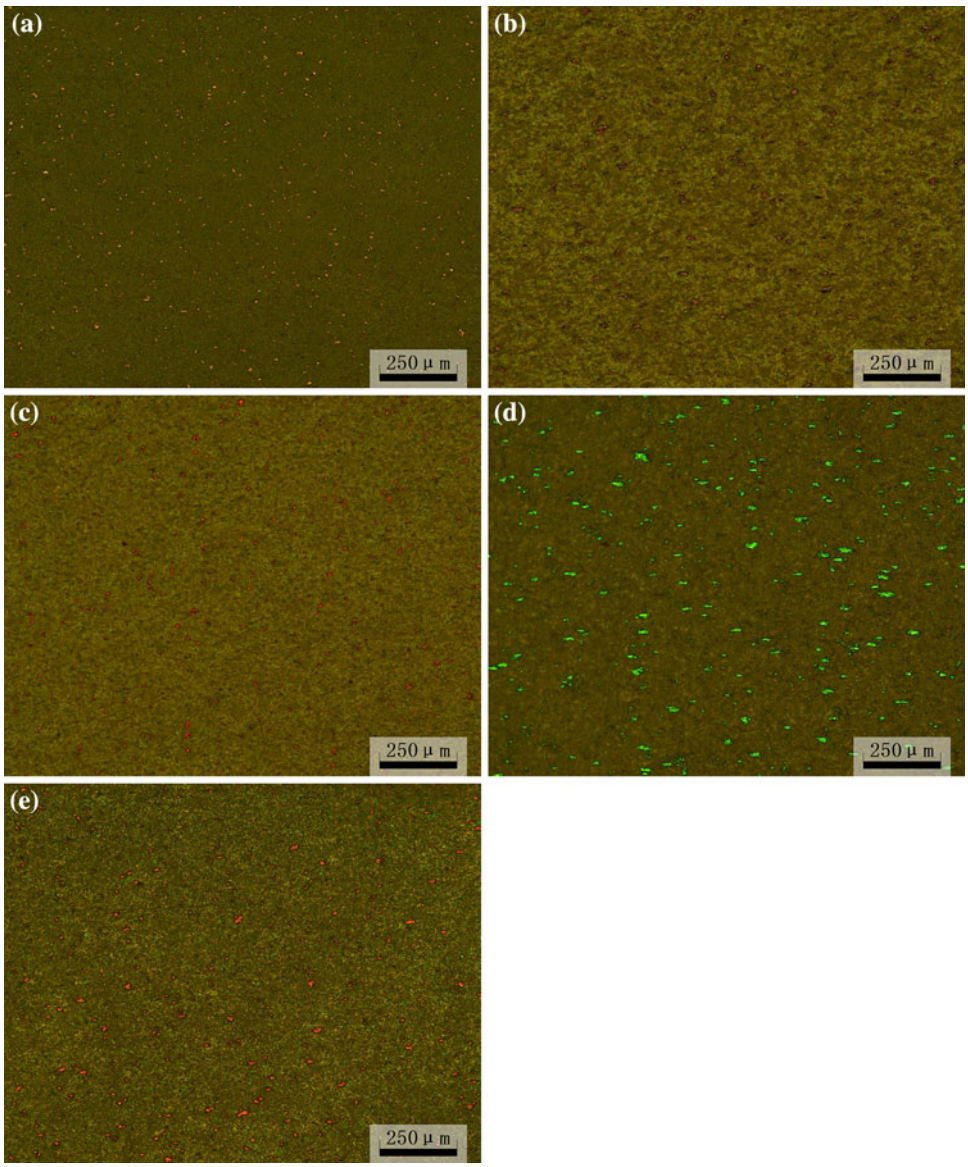

Fig. 3 OM images of specimens at various electrolyte concentrations: **a** 1 g L^{-1}; **b** 3 g L^{-1}; **c** 5 g L^{-1}; **d** 10 g L^{-1}; **e** 15 g L^{-1}

electrolyte concentration until it reached the maximum at 5 g L^{-1}. Thereafter, the intensity decreased with electrolyte concentration. The appearance of the broad bands (405–434 and 607–641 cm^{-1}) might be attributed to the effect of impurity doping, defects and strains introduced from pretreatment process [15].

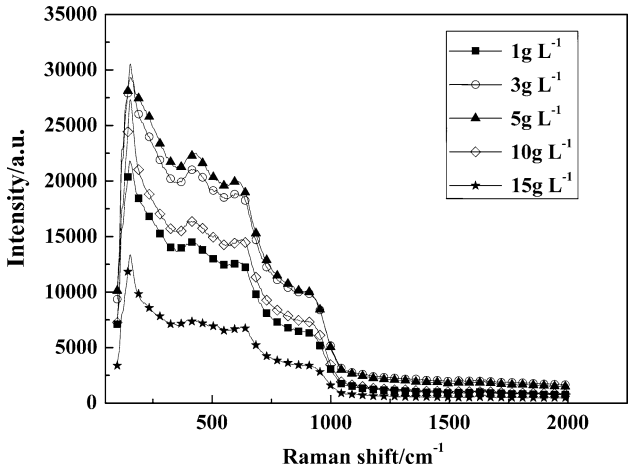

Fig. 4 Raman spectra of anodic oxide films formed on titanium alloy Ti-10V–2Fe–3Al at various electrolyte concentrations

3.4 Electrochemical behaviors of specimens at various electrolyte concentrations

The Nyquist plots of the specimens at various electrolyte concentrations are shown in Fig. 5. Two semicircles, which were respectively associated with compact inner layer and porous outer layer, were observed on the specimens at various electrolyte concentrations. The diameter of the semicircle initially increased with electrolyte concentration until it reached the maximum at 5 g L^{-1}. Thereafter, the diameter decreased with electrolyte concentration. It was obvious that the semicircles turned to be straight lines with the slope approaching 1 at low frequency, which was a symbol for diffusion.

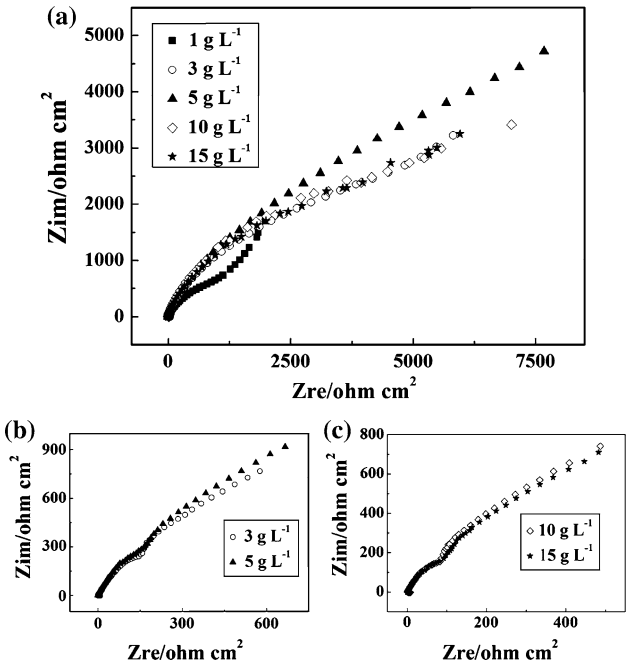

Fig. 5 Nyquist plots of specimens at various electrolyte concentrations (**a**); enlargement of plots of specimens at 3 and 5 g L^{-1} (**b**); enlargement of plots of specimens at 10 and 15 g L^{-1} (**c**)

Figure 6 shows the Bode plots (log |Z| vs. log f) of the specimens at various electrolyte concentrations. Straight lines were observed with the slope approaching −1 in frequency region (10^0–10^{-2}). The maximum absolute value of impedance (|Z|) exhibited the same rule as that obtained from Nyquist plots. The |Z| value firstly increased

Table 4 Raman peaks of anodic oxide films formed on titanium alloy Ti-10V–2Fe–3Al at various electrolyte concentrations

Electrolyte concentration (g L^{-1})	Wave number of Raman peaks tested (cm^{-1})	Wave number of Raman peaks reported in literature (cm^{-1})	Microstructures corresponding to the Raman peaks
1	152	Eg mode 147	Anatase
	417	E1g mode 399	Anatase
	635	Eg mode 640	Anatase
3	152	Eg mode 147	Anatase
	434	Eg mode 445	Rutile
	607	A1g mode 607	Rutile
5	152	Eg mode 147	Anatase
	428	Eg mode 445	Rutile
	618	A1g mode 607	Rutile
10	152	Eg mode 147	Anatase
	422	Eg mode 445	Rutile
	624	Eg mode 640	Anatase
15	152	Eg mode 147	Anatase
	405	E1g mode 399	Anatase
	641	Eg mode 640	Anatase

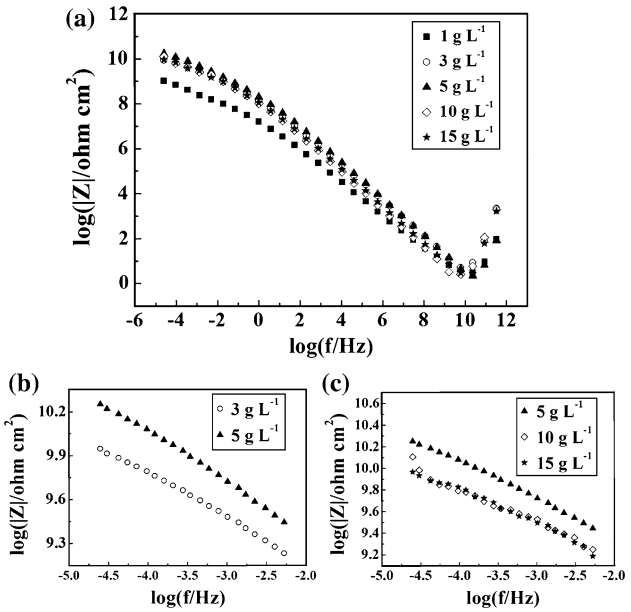

Fig. 6 Bode plots (log |Z| vs. log f) of specimens at various electrolyte concentrations (**a**); enlargement of plots of specimens at 3 and 5 g L^{-1} (**b**); enlargement of plots of specimens at 5, 10 and 15 g L^{-1} (**c**)

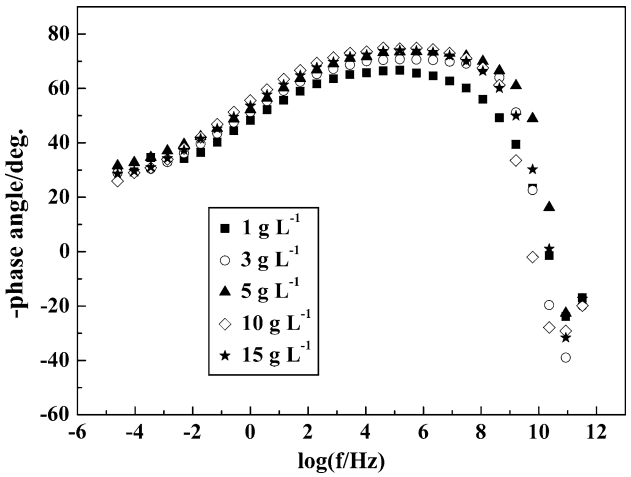

Fig. 7 Bode plots (-phase angle vs. log f) of specimens at various electrolyte concentrations

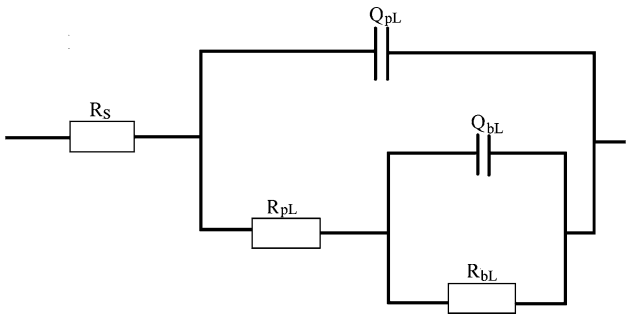

Fig. 8 Equivalent circuit diagram for specimens at various electrolyte concentrations

with electrolyte concentration until it came to the maximum at 5 g L^{-1}. Thereafter, the value decreased with electrolyte concentration.

The Bode plots (-phase angle vs. log f) of the specimens at various electrolyte concentrations are presented in Fig. 7. The phase angle increased with the decrease of the frequency in the higher-frequency region (10^5–10^4) and remained constant in the intermediate frequency (10^4–10^1). A highly capacitive behavior, typical of passive materials, is indicated by phase angles approaching −90°, suggesting that a highly stable film is formed on the surface [16]. Therefore, the phase angles which were closed to −90° in the middle-frequency region (10^4–10^1) exhibited a near-capacitive response. In the lower-frequency region (10^1–10^{-2}), the phase angle gradually decreased with the decrease of the frequency. The phase angle showed little difference at various electrolyte concentrations.

The equivalent circuit model $R_S(Q_{pL}(R_{pL}(Q_{bL}R_{bL})))$ [17] for specimens at various electrolyte concentrations is shown in Fig. 8. Where, R_S is the solution resistance, R_{pL} is the polarization resistance of the porous layer, Q_{pL} is the capacitance of the porous layer, R_{bL} is the polarization resistance of the barrier layer and Q_{bL} is the capacitance of the barrier layer. A constant-phase element CPE representing a shift from the ideal capacitor was used instead of the capacitance. The impedance of the constant-phase element (Z_{CPE}) is defined by Eq. 1 [18],

$$Z_{CPE} = [Q(j\omega)^n]^{-1} \quad (1)$$

where, Q is the magnitude of CPE, ω is the angular frequency and n is the exponent of CPE, with values between −1 and 1.

The polarization resistance, capacitance and n values of the specimens at various electrolyte concentrations were obtained by adjusting the experimental data to the equivalent circuit. Those values are given in Table 5. Fitting error are less than 10%, which indicated that the data adjusted well to the proposed equivalent circuit.

A true capacitive behavior has a value of $n = 1$, and is rarely obtained. The difference between n value and 1 represents the deviation from an ideal capacitor. According to the data in Table 5, the n_p values of the specimens at various electrolyte concentrations were close to 1, which meant the porous layers of all the films were approximately ideal capacitors. The n_b values of the specimens at various electrolyte concentrations were close to each other, which meant such values had unessential influence on the differences among film impedances.

According to Fig. 8, the electrochemical impedances for the specimens at various electrolyte concentrations are given by Eq. 2,

Table 5 AC impedance parameters for specimens at various electrolyte concentrations

Electrolyte concentration (g L^{-1})	R_S (Ω cm^2)	R_{pL} (Ω cm^2)	Q_{pL} (μF cm^{-2})	n_p	R_{bL} ($k\Omega$ cm^2)	Q_{bL} (μF cm^{-2})	n_b	χ^2
1	3.696	29.46 (±2.5)	14.56 (±1.7)	0.9863	73.63 (±9.7)	175.3 (±13)	0.5589	2.401×10^{-3}
3	10.23	89.64 (±9.6)	2.597 (±0.3)	0.9829	128.9 (±11)	634.8 (±38)	0.5712	1.229×10^{-3}
5	3.411	33.85 (±3.1)	5.988 (±0.7)	0.9910	182.2 (±14)	503.5 (±32)	0.5820	1.773×10^{-3}
10	10.54	101.3 (±10)	11.15 (±1.2)	0.9903	178.9 (±13)	667.2 (±40)	0.5633	1.913×10^{-3}
15	10.11	93.52 (±9.7)	12.34 (±1.4)	0.9872	165.5 (±12)	713.9 (±42)	0.5581	1.805×10^{-3}

$$Z = R_s + \frac{1}{\frac{1}{Z_{pLCPE}} + \frac{1}{R_{pL} + \frac{1}{\frac{1}{R_{bL}} + \frac{1}{Z_{bLCPE}}}}} \tag{2}$$

where Z_{pLCPE} is the impedance of the constant-phase element of the porous layer, Z_{bLCPE} is the impedance of the constant-phase element of the barrier layer.

Z_{CPE} in Eq. 1 is inserted to Eq. 2, and the electrochemical impedances of the specimens at various electrolyte concentrations are calculated and shown by Eq. 3,

$$Z = R_s + \frac{1}{(j\omega)^{n_p} Q_{pL} + \frac{1}{R_{pL} + \frac{1}{\frac{1}{R_{bL}} + (j\omega)^{n_b} Q_{bL}}}} \tag{3}$$

According to Eq. 3, the impedances of the specimens at various electrolyte concentrations increase with the increase of polarization resistances (R_{pL}, R_{bL}) and the decrease of capacitances (Q_{pL}, Q_{bL}).

As shown in Table 5, the capacitances of porous layer and barrier layer (Q_{pL} and Q_{bL}) initially decreased with electrolyte concentration until they reached the minimum at 5 g L^{-1}. Thereafter, Q_{pL} and Q_{bL} increased with electrolyte concentration. On the other hand, the polarization resistances of porous layer and barrier layer (R_{pL} and R_{bL}) firstly increased with electrolyte concentration until they reached the maximum at 5 g L^{-1}. Then R_{pL} and R_{bL} decreased with electrolyte concentration.

Therefore, the impedance of specimen initially increased with electrolyte concentration until it reached the maximum at 5 g L^{-1}. Thereafter, the impedance decreased with electrolyte concentration.

4 Discussion

The linear increase of anodizing forming voltage in step (1) has been explained by the well-known high field-assisted ionic transport mechanism [19, 20]. The relationship between the anodic current and the electric field strength across the anodic oxide film is described by the following Eq. 4 [21],

$$i = A \exp(BE) \tag{4}$$

where i is the ionic current, A and B are the electrolytic constants, E is the electric field strength and can be replaced by V/δ, where V is the anodizing forming voltage and δ refers to the anodic oxide thickness. During galvanostatic anodizing, in order to maintain the given constant current density, constant field strength across the previously formed barrier film is required. As a consequence, when the oxide thickness increases with time at constant current density, the voltage across the oxide film must increase in order to maintain the field strength and the current density. As shown in Fig. 2, our experimental data presented evidently the linear increase of the anodizing forming voltage in step (1). This is well consistent with the above equation. Hence, so far as anodic oxide thickness of barrier film is concerned, the following equations can be induced [6],

$$\delta = \alpha V \tag{5}$$

$$\frac{d(\delta)}{dt} = \alpha \frac{d(V)}{dt} \tag{6}$$

where α is the growth constant. The growth constant α is related to the nature of electrolyte solution [6]. In case of a certain electrolyte solution, the raising rate of anodizing forming voltage in step (1) can be used to express the oxide film formation rate.

It is generally assumed that the anodic oxide growth behavior is determined by electrochemical dynamics between the formation ability of the oxide film and the dissolution ability of the electrolyte solution. The presence of the maximum value of anodizing forming voltage in step (2) (presented in Table 4) can be explained on the basis of this dynamic equilibrium. The anodizing forming voltage goes up when the rate of oxide film formation exceeds the dissolution rate. The film grows thicker with the time, which suppresses the film formation. Therefore, after a few minutes of anodizing, the rate of oxide film formation is lower than the rate of chemical dissolution, which leads to the decrease of the anodizing forming voltage. Corresponding to the steady step (3), dynamic equilibrium between the

oxide formation rate and chemical dissolution rate is established.

Theoretically, it has been proposed that during electrochemical anodizing, the 'electrical double layer' forms at the oxide film/electrolyte interface, which consists of an excess or deficit of electrons on the metal side and of an excess or deficit of ions on the electrolyte side [10]. These couplings of electrons and ions during anodizing normally result in a certain gradient of the concentration distribution of the electrolyte at the oxide film/electrolyte interface. In this situation, if an increase of the electrolyte concentration is sufficient to heighten the lowered concentration of the inner layer, the electrochemical reaction at the interface accelerates and then the electrical resistance will be reduced. Eventually the anodizing forming voltage decreases with the increase of the electrolyte concentration [6]. This theory can be demonstrated by the decrease of the ultimate value of anodizing forming voltage in step (3) (shown in Table 4) with electrolyte concentration.

The coloring of the passive oxide film formed on breakdown points can be explained by the multiple beam interference theory. When the light source from optical microscopy strikes the titanium oxide, there will be an interference phenomenon between the reflected beam from the oxide surface and the beam which penetrates the surface oxide and then it reflected from the interface of the surface oxide and titanium substrate. Therefore, interference colors can be affected by anodic oxide thickness, and the thickness of the passive film was in relation to the ultimate value of anodizing forming voltage. This is in good agreements with previous literature [22]. The porous layers of anodic oxide films formed at various electrolyte concentrations exhibited the same color, which was with respect to the good visible-light absorbance of carbon in the films [13, 23].

The surface morphology, microstructure and electrochemical impedance of anodic oxide film were strongly dependent upon electrolyte concentration in terms of the change rate of anodizing forming voltage.

In the electrolyte solutions with lower concentration, for example at 1 g L^{-1}, the dissolution ability of electrolyte solution was weak and the oxide film formation rate extremely exceeded the chemical dissolution rate. Therefore, anodic oxide film grew at a high rate of 24.8 V min^{-1}. The compact layer of oxide film formed in a short time and suppressed porous layer formation. Consequently, the anodizing forming voltage decreased slowly. As shown in Fig. 2, the steady step kept only 4 min at 1 g L^{-1}. The thinnest outer layer of oxide film at 1 g L^{-1} was related to such short time of step (3).

With the increase of electrolyte concentration, the dissolution ability of electrolyte solution was heightened. Therefore, the change rate of anodizing forming voltage decreased, companied by improving the uniformity of the oxide film, increasing the amount of crystal phase and enhancing the electrochemical impedance of the oxide film.

In electrolyte solution with higher concentration, i.e. 10 and 15 g L^{-1}, the change rate of anodizing forming voltage increased again, which may be associated with the electrolyte ions incorporated into anodic oxide films [13]. The largest breakdown points observed on the oxide film formed at 10 g L^{-1} were ascribed to the extremely large falling rate of anodizing forming voltage of 11.6 V min^{-1}. The fast decrease may be attributed to abnormal chemical dissolution by electrolyte.

5 Conclusions

Surface morphology, microstructure and electrochemical impedance of anodic oxide film were remarkably dependent upon electrolyte concentration in terms of the change rate of anodizing forming voltage. In fact, the increase of electrolyte concentration initially led to more uniform surface, larger amount of crystal phase and greater electrochemical impedance by decreasing the change rates of anodizing forming voltage, whereas after a certain concentration (5 g L^{-1}), electrolyte concentration affected those characteristics oppositely.

When electrolyte concentration was 5 g L^{-1}, anodic oxide film was the most uniform, exhibited by the least and smallest breakpoints on the film. In addition, the amount of crystal phase of the film was the largest at 5 g L^{-1}, showed by the highest intensity of Raman peaks. Furthermore, the electrochemical impedance of the film of the alloy was the greatest at 5 g L^{-1}, demonstrated by the highest values of polarization resistances and lowest values of capacitances. These phenomenon were associated with the minimum value of the change rate of anodizing forming voltage at 5 g L^{-1}.

Acknowledgement This article is supported by the fundamental research funds for the central universities.

References

1. Boyer RR (1996) An overview on the use of titanium in the aerospace industry. Mater Sci Eng A 213:103
2. Popa MV, Vasilescu E, Drob P, Anghel M, Vasilescu C, Rosca IM, Lopez AS (2002) Anodic passivity of some titanium base alloys in aggressive environments. Mater Corros 53:51
3. Wang B, Liu ZQ, Gao Y, Zhang SZ, Wang XY (2007) Microstructural evolution during aging of Titanium alloy Ti-10V–2Fe–3Al. J Univ Sci Technol Beijing 14:335
4. Fovet Y, Gal JY, Chemla FT (2001) Influence of pH and fluoride concentration on titanium passivating layer stability of titanium dioxide. Talanta 53:1053
5. Diamanti MV, Pedeferri MP (2007) Effect of anodic oxidation parameters on the titanium oxides formation. Corros Sci 49:939

6. Sul YT, Johansson CB, Jeong Y, Albrektsson T (2001) The electrochemical oxide growth behavior on titanium in acid and alkaline electrolytes. Med Eng Phys 23:329
7. Kalra KC, Singh KC, Singh M (1997) Formation and breakdown characteristics of anodic oxide films on valve metal. Indian J Chem 36:216
8. Dyer CK, Leach JSL (1978) Breakdown and efficiency of anodic oxide growth on titanium. J Electrochem Soc 125:1032
9. Delplancke JL, Winand R (1988) Galvanostatic anodization of titanium—II. Reactions efficiencies and electrochemical behavior model. Electrochim Acta 33:1551
10. Sato N (1971) A theory for breakdown of anodic oxide films on metals. Electrochim Acta 16:1683
11. Shibata T, Zhu YC (1995) The effect of temperature on the growth of anodic oxide film on titanium. Corros Sci 37:133
12. Liu JH, Yi JL, Li SM, Long GR, Gan WK (2007) Anodic oxidizing process of titanium alloys in ammonium tartrate electrolyte. Chinese Patent CN 1908245A
13. Liu JH, Yi JL, Li SM, Yu M, Xu YZ (2009) Fabrication and characterization of anodic oxide films on titanium alloy Ti-10V–2Fe–3Al. Int J Miner Met Mater 16:96
14. Pan XY, Ma XM (2001) Progress of research on Raman spectra of nano-TiO_2. Mater Sci Eng (in Chinese) 19:138
15. Wang J, Zhang QW, Yin S, Sato T, Saito F (2007) Raman spectroscopic analysis of sulphur-doped TiO_2 by co-grinding with TiS_2. J Phys Chem Solids 68:189
16. Tamilselvi S, Raman V, Rajendran N (2006) Corrosion behavior of Ti–6Al–7Nb and Ti–6Al–4V ELI alloys in the simulated body fluid solution by electrochemical impedance spectroscopy. Electrochim Acta 52:839
17. Assis SL, Wolynec S, Costa I (2006) Corrosion characterization of titanium alloys by electrochemical techniques. Electrochim Acta 51:1815
18. Shukla AK, Balasubramaniam R (2006) Effect of surface treatment on electrochemical behavior of CP Ti, Ti–6Al–4V and Ti–13Nb–13Zr alloys in simulated human body fluid. Corros Sci 48:1696–1720
19. Vermilyea DA (1953) The kinetics of formation and structure of anodic oxide films on tantalum. Acta Met 1:282
20. Young L (1954) Anodic oxide films on tantalum electrodes. Trans Faraday Soc 50:159
21. Ammar IA, Kamal I (1971) Kinetics of anodic oxide-film growth on titanium—I. Acid media. Electrochim Acta 16:1539
22. Delplancke JL, Degrez M, Fontana A, Winand R (1982) Self-colour anodizing of titanium. Surf Coat Technol 16:153
23. Kuo CS, Tseng YH, Huang CH, Li YY (2007) Carbon-containing nano-titania prepared by chemical vapor deposition and its visible-light-responsive photocatalytic activity. J Mol Catal A: Chem 270:93